Polaritonic Bright and Dark States Collectively Affect the Reactivity of a Hydrolysis Reaction

Yulei Wang,[1,2] Daniel Rosenmann,[1] John V. Muntean,[3] and Xuedan Ma[1,4]*

[1]Center for Nanoscale Materials, Argonne National Laboratory, Lemont, Illinois 60439, United States

[2]Consortium for Advanced Science and Engineering, University of Chicago, Chicago, Illinois 60637, United States

[3]Chemical Sciences and Engineering, Argonne National Laboratory, Lemont, Illinois 60439, United States

[4]Department of Materials Science and NanoEngineering, Rice University, Houston, Texas, 77005, United States

ABSTRACT

Vibrational strong coupling (VSC) has emerged as a means for modifying chemical reactivity. Despite the intriguing discoveries and progresses in the field, the precise mechanisms that govern polaritonic chemistry still deserve further interrogation. Herein, we use the hydrolysis of ammonia

borane in D_2O as an exemplary reaction and systematically investigate the influence of VSC on its reactivity. Experimental evidence of the coexistence of a resonant effect and reaction acceleration is observed in this system. In particular, we find that when the O-D stretching mode of D_2O is strongly coupled to a cavity mode, reaction acceleration is observed. The reaction rate acceleration factor, μ, is consistently observed to be dependent on the coupling conditions between the vibrational and cavity modes, and reaches a minimum at zero mode detuning, suggesting that a resonant effect is likely in play. In addition, we find that μ decreases with increasing Rabi splitting. Based on these experimental findings, we propose that the overall influence of VSC on the reactivity of this reaction is likely determined collectively by the polaritonic bright and dark states. These findings could help shed new light on the intricate effects of VSC on ground-state reaction landscapes.

Keywords: vibrational strong coupling, Rabi splitting, ground-state reaction, resonant effect, polaritonic dark state

TOC

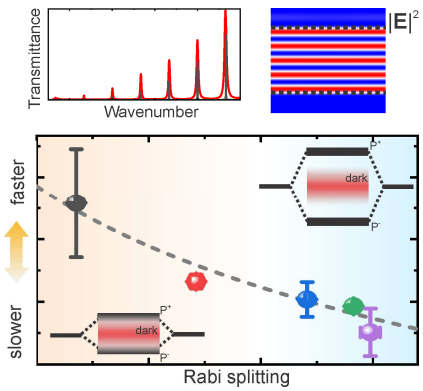

INTRODUCTION

To overcome limitations imposed by the naturally small value of the fine structure constant,[1] structured local electromagnetic fields have been widely used to modify the interaction strength of a dipole with light.[2] When the interaction between the dipole and photons occurs at a rate faster than the dissipation rates of the system, it enters the strong coupling regime, in which new eigenstates called cavity polaritons are formed. The realization of strong coupling in solid state systems such as semiconductors and superconductors has enabled the observation of numerous exotic phenomena such as polariton condensation and superfluidity,[3, 4] photon blockade,[5, 6] extreme nonlinear optics,[7-9] and long-distance energy transfer.[10, 11]

In a concurrent manner, applying strong coupling to molecular systems has the potential to transform contemporary chemistry.[12, 13] Selective coupling of molecular electronic and vibrational transitions with cavity photons has been demonstrated to alter chemical reaction rates and selectivity.[14-22] These fascinating experimental discoveries have inspired many theoretical models to explain the results and provide further guidance.[23-31] However, on account of the complexity of the systems, precise principles underpinning polaritonic chemistry still remain inconclusive. Strong coupling between a cavity mode and N molecular transitions gives rise to two bright polaritonic states that are delocalized over all the resonant molecules, as well as N-1 dark states with energy distributions resembling those of the bare molecules.[32-34] It still remains to be elucidated what exact roles the polaritonic bright and dark states play, and how they conjointly affect the chemical landscapes. In particular, theoretical models have yet to reconcile with the experimental observations of both reaction rate acceleration[19, 35] and deceleration[17, 18, 20, 21] in adiabatic reactions upon resonant vibrational strong coupling (VSC). For instance, theoretical studies based on the dynamical caging effect[36, 37] and quantum electrodynamical density functional

method[38] have predicted trapped reaction coordinates and trajectories, as well as reduced reaction rates, while theoretical models considering vibrational dissipation via dark states[39, 40] support the scenario of accelerated reaction rates.[39] Moreover, compared to solid-state systems, a comprehensive understanding of liquid phase reactions can be further thwarted by the unavoidable molecular rotations and intermolecular collisions that change the instant dipole orientations and thermodynamic states of the systems.[40] As such, experimental works that could help disentangle these intertwined effects and shed light on the fundamental mechanisms are highly desirable.[23]

Here, we provide experimental evidence that could help elucidate the concurrent influence of polaritonic bright states and the thermalization effect on reaction rates. Specifically, we investigate a hydrolysis reaction, in which the vibrational mode of a reactant, D_2O, is strongly coupled to a cavity mode. We find the reaction rate to be closely related to the overlap between the polaritonic dark and bright states, which is intricately determined by the Rabi splitting and mode detuning: at a large overlap facilitated by reducing the Rabi splitting and/or increasing the mode detuning, larger acceleration in the reaction rate is observed. In contrast, a reduction in the overlap between the polaritonic dark and bright states results in smaller acceleration. These findings suggest that in the currently studied system, both resonant effect and dark state-associated thermalization play critical roles in determining the overall reaction rates.

RESULTS AND DISCUSSION

Reaction and strong coupling conditions

Fabry-Pérot (FP) cavities are used in this study to provide quantized electromagnetic fields in the vertical directions of the cavities (Figure 1b inset).[41] Mode frequencies of FP cavities follow $\omega_0 = m/(2nL)$, with m being the mode order, n the filling medium refractive index, and L the cavity length. By adjusting the cavity length, the FP cavity modes can be continuously tuned over a certain frequency range. Each of the cavities used in this study consists of two parallel Au mirrors separated by an approximately 6 μm thick Mylar spacer. They are assembled in a commercial FTIR flow cell following a previously reported method.[17, 18] The Au mirrors are fabricated by subsequently depositing 10 nm of Au, 2 nm of Cr, and a 100 nm passivation layer of SiO_2 onto calcium fluoride (CaF_2) windows (see Methods and Figure S1 for experimental details). Figure 1b shows a representative FTIR transmission spectrum of an as-assembled empty cavity, whose mode frequencies can be well reproduced by numerical simulations. The broader linewidths (and hence smaller quality factors) observed in the experimental spectra compared to those from the numerical simulations are likely associated with surface roughness-induced imperfections in the Au mirrors, influences of the substrates and passivation layers, and/or imperfect alignment of the two Au mirrors. We would like to note that the 6 μm-thick spacer is chosen primarily for two reasons: i) to ensure that there are sufficiently large free spectral ranges (~ 660 cm^{-1}) for accommodating our mode detuning-dependent studies, and ii) to avoid unintentional coupling of a designated vibrational mode with multiple cavity modes.

In this study, we consider the hydrolysis reaction of ammonia borane (NH_3BH_3) in deuterium water (D_2O), the influence of VSC on which has raised much interest and remains inconclusive.[42, 43] Aside from providing additional experimental evidence that could contribute to the understanding of this types of reactions and shed light on any unveiled mechanisms that may have led to inconsistencies in previous reports, we choose this reaction to study also because it allows us to

systematically investigate several important VSC metrics in the same system: Firstly, due to the broad O-D stretching mode in D_2O (ω_0 ~ 2500 cm^{-1}, Figure 1c blue peak), a wide range of overlap degrees between the polaritonic bright and dark states can be achieved by adjusting the mode detuning and coupling strength conditions (vide infra). Secondly, to avoid complications, the vibrational mode is set to be coupled to only one cavity mode instead of multiple ones. The amplitude and frequency of the transition dipole moment of the O-D stretching mode ensure that various VSC strengths manifested as Rabi splitting values can be achieved by simply adjusting the D_2O concentrations. These two characteristics of this reaction system allow us to study the intricate influences of the bright and dark states through a series of reaction conditions.

The hydrolysis reaction has D_2O and NH_3BH_3 as the reactants, and isopropanol (IPA) as the reagent (Figure 1a). Detailed compositions of the products are determined from NMR measurements (Figure S2). Here, IPA is chosen as the reagent due to its relatively similar solvent polarity compared to D_2O (0.546 for IPA vs 0.991 for D_2O),[44] and lack of strong absorption bands in the frequency window that is of interest to this study. The concentration of D_2O, [D_2O], in the initial mixture is tuned between 10% to 50% of the total volume (V_0) for reasons that will be explained below. For clarity, the concentration of D_2O is simply labeled using its volume percentage ([D_2O] = nV_0, n = 0.1 – 0.5) in the following text. In all the reactions studied here, the initial concentration of NH_3BH_3 is kept the same, namely 1 M.

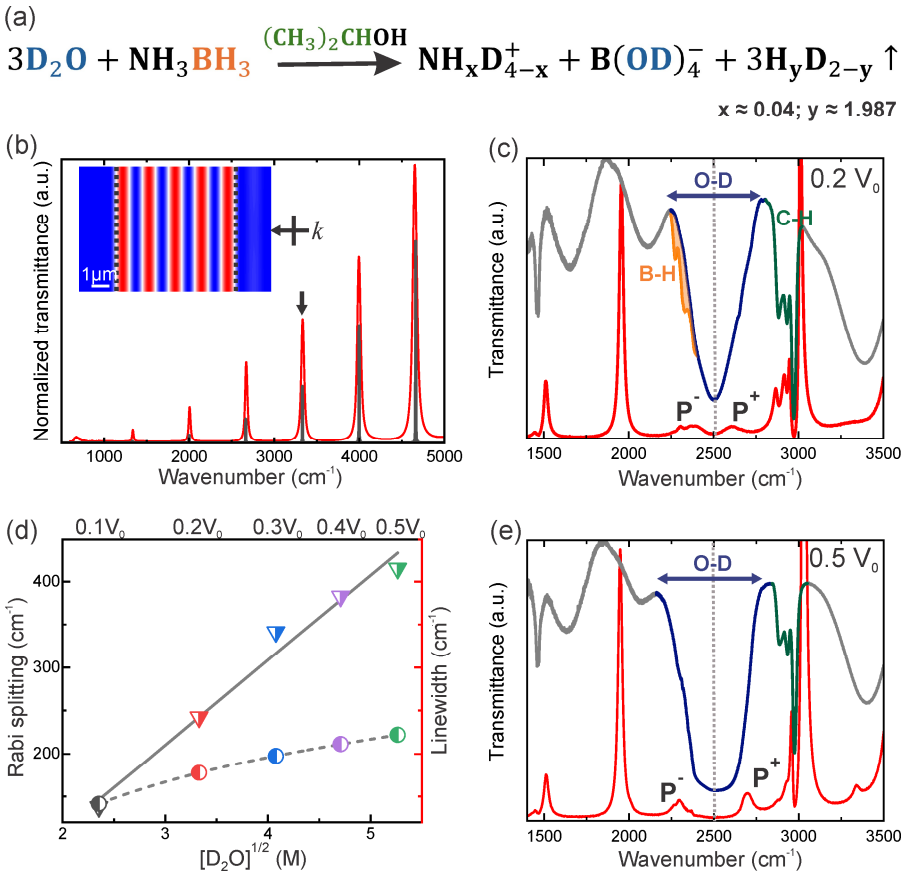

Figure 1. (a) Hydrolysis of ammonia borane in a mixture of D_2O and IPA. (b) A representative IR transmission spectrum of an empty cavity (red) and the corresponding simulated spectrum for an empty cavity with a cavity length L = 7.5 μm (black). Inset: electric field intensity ($|\mathbf{E}|^2$) distribution inside the empty cavity for the m = 5 mode as indicated by an arrow in the transmission spectrum. Positions of the Au mirrors are marked by the dashed lines. (c) Top curve: IR transmission spectrum of a mixture of $0.2V_0$ D_2O and $0.8V_0$ IPA. The O-D stretching mode in D_2O (~ 2500 cm^{-1}), C-H stretching mode in IPA (~ 2970 cm^{-1}), and B-H stretching mode (~ 2250 – 2380 cm^{-1}) in NH_3BH_3 are color coded in blue, green, and orange, respectively. Red curve: IR transmission spectrum of the $0.2V_0$ D_2O, $0.8V_0$ IPA, and NH_3BH_3 mixture when the O-D stretching mode at ~ 2500 cm^{-1} is strongly coupled to a cavity mode. (d) Rabi splitting (triangle) and spectral linewidth of the O-D stretching mode (circle) at various concentrations of D_2O. The linewidths are calculated from absorbance spectra. The solid line is a linear fit, while the dashed line is a guide to the eye. (e) Top curve: IR transmission spectrum of a mixture of $0.5V_0$ D_2O and $0.5V_0$ IPA. Red curve: IR transmission spectrum of the $0.5V_0$ D_2O, $0.5V_0$ IPA, and NH_3BH_3 mixture when the O-D stretching mode is strongly coupled to a cavity mode.

In a typical experiment, the cavity length is fine-tuned by adjusting the screws on the flow cell, and the $m = 5$ cavity mode is used to couple to the O-D stretching mode. When the cavity mode is tuned into resonance with the vibrational mode (*i.e.* detune $\Delta_0 \approx 0$), the original cavity peak splits into a pair of lower (P^-) and upper (P^+) polaritonic states (Figure 1c, red). The peak shape of P^- is slightly irregular due to the additional B-H stretching mode from NH_3BH_3 in the frequency range of ~ 2250 – 2380 cm^{-1} (Figure 2c, orange). The influence of the B-H mode on the reactivity is expected to be minimal due to its detuned frequency from microcavity modes and more importantly, the low concentrations of NH_3BH_3 used in this study.

As shown in Fig. 1d (circles), an increase in the D_2O concentration leads to a slight broadening of the O-D stretching mode, which is likely related to an increased occurrence of hydrogen bonding at high D_2O concentrations.[45, 46] In parallel, the Rabi splitting value also increases, exhibiting a linear dependence on the square root of [D_2O] (Figure 1d triangles). Overall, we consider reactions with D_2O concentrations in the range between $0.1V_0$ and $0.5V_0$ to be in the strong coupling regime, because their Rabi splitting values are larger than the corresponding FWHMs of the O-D vibrational modes and the cavity modes. For instance, we obtain a Rabi splitting of $\Omega = 242$ cm^{-1} for the $0.2V_0$ D_2O reactions, which is larger than the corresponding FWHM of the O-D vibrational mode (178 cm^{-1}, Figure 1d red circle) and the cavity mode, confirming the interaction to be in the strong coupling regime. We use $0.1V_0$ as the lower limit of the D_2O concentration, since the corresponding Rabi splitting (138 cm^{-1}) and FWHM of the O-D vibrational mode (141 cm^{-1}) are close to each other, hence placing this condition to be at the crossover from the weak to the strong coupling regimes. A further reduction in the D_2O concentration would place the system in the weak coupling regime, and no polaritonic states would be formed. On the other hand, it is worth

mentioning that at $0.5V_0$, the ratio η between the coupling strength ($g = \Omega/2$) and the O-D vibrational frequency (ω_0) is 0.083, approaching the condition of η = 0.1, which defines the onset of the ultrastrong coupling regime. Overall, by controlling the D_2O concentration in the reaction system, we are able to adjust the strong coupling condition.

Quantification of reaction rates

Due to the large excess of D_2O compared to ammonia borane in the reactant mixture, pseudo-first-order kinetics are expected. In principle, reaction time-dependent absorbance change of the reactants can be used for calculating the rates of this kind of pseudo-first order reactions, because the absorbance of the reactants' vibrational modes is directly proportional to their concentrations inside the cavity.[43] However, due to the varying reflectivity of the microcavity over the course of a reaction,[43] and the spectral overlap between the reactants' vibrational modes and cavity modes, accurate determination of reactant absorbance change as a function of reaction time is challenging. As such, we primarily use cavity mode shifts for the estimation of the reaction rates.

Progress of the reactions is monitored by recording the reaction time-dependent IR transmission spectra (see Figure 2a for an exemplary case and Methods for experimental details). Upon injection of the two reactants, i.e. D_2O and NH_3BH_3, and the reagent IPA into a cavity, continuous blue shifts in the cavity modes can be observed during the reactions (Figure 2b). In stark contrast, injecting mixtures of D_2O and IPA only into a cavity without the other key reactant NH_3BH_3 yields no apparent peak shift (Figure S3), confirming that the blue shifts in the IR transmission spectra are associated with the reactions inside the cavities rather than issues such as cavity stability and

sealing, etc. The slightly smaller refractive index of the product compared to the reactant could account for this cavity mode shift.[17, 20]

A detailed description of the approach for deriving reaction rates from cavity mode shifts is provided in Supporting Information S1. In principle, the following correlation between the cavity resonance frequency $\omega_c(t)$ at time t, and the average reaction rate k over a specific period of reaction time can be obtained:

$$\ln \omega_c(t) \propto -\ln [\exp(-kt) + C]$$

Here, C is a constant related to the refractive indices of the reactants and products. By plotting $\ln \omega_c(t)$ as a function of the reaction time t, and fitting the experimental data with the above equation, the average reaction rate k can be derived. In general, a larger initial slope indicates a faster reaction (Figure S4). Indeed, we find that this equation can well describe the reaction time-dependent mode shifts, as shown in Figure 2c. For the exemplary reaction with an initial detuning value of $\Delta_0 \approx 0$ shown in Figure 2a and 2b middle, a k value of 2.39×10^{-4} min^{-1} can be obtained (Figure 2c, red dots and line). Also, similar reaction rates can be obtained when different cavity modes were used for analysis (Figure S5). We would like to note that due to the broad linewidth of the O-D vibrational mode, the definition of mode detuning is less apparent in this system. For clarity, we refer to the energy difference between the cavity mode peak and the O-D mode peak as the detuning value. Applying a similar approach to reactions with large mode detuning values at the beginning of the reaction, we observe more drastic peak shifts (see e.g. Figure 2b and 2c for reactions with Δ_0 = -126.6 cm^{-1} and Δ_0 = 76.6 cm^{-1}). k values of 7.21×10^{-4} min^{-1} for Δ_0 = -126.8 cm^{-1} (black dots) and 4.41×10^{-4} min^{-1} for Δ_0 = 76.6 cm^{-1} (blue dots), respectively, are obtained by applying the fitting method described above. Based on this fitting approach, it is potentially

conceivable to develop a verification method that relies on injecting mixtures consisting of reaction products with known concentrations (and hence refractive indices) into the cavities and monitor whether the cavity mode frequencies match with those from the in-situ measurements.

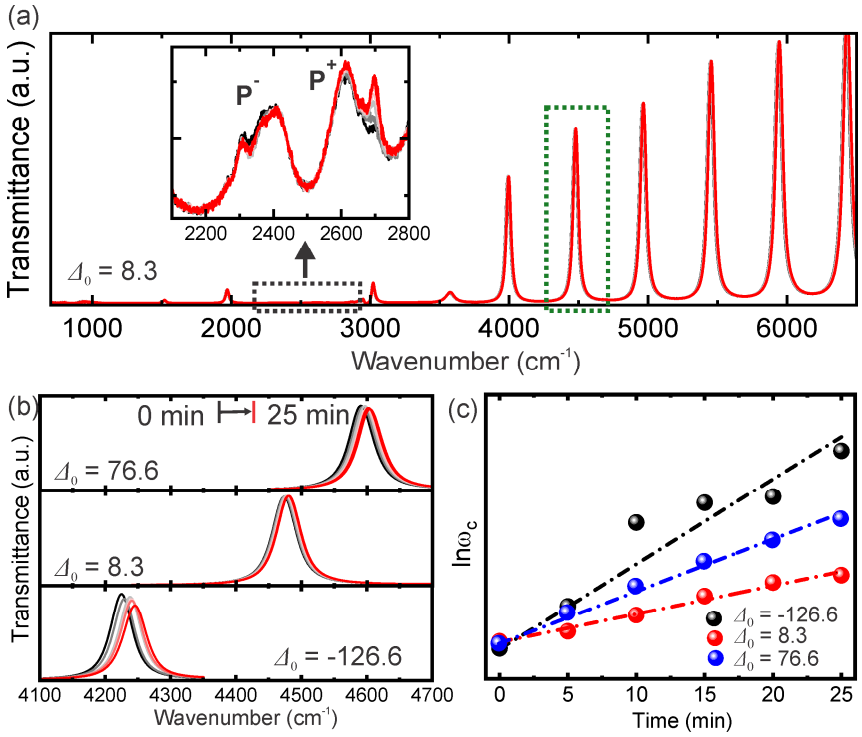

Figure 2. (a) Reaction time-dependent IR transmission spectra of a mixture of 1 M ammonia borane, $0.2V_0$ D_2O, and $0.8V_0$ IPA for an inside-cavity experiment with $\Delta_0 \approx 0$. Inset: zoomed-in view of the $m = 5$ cavity mode. The region marked by a green rectangle corresponds to the data in (b) middle row. (b) Shifts in the $m = 9$ cavity mode as a function of the reaction time for inside-cavity experiments with $\Delta_0 > 0$ (top), $\Delta_0 \approx 0$ (middle), and $\Delta_0 < 0$ (bottom). (c) Reaction time-dependent ln ω_c values for the three cases shown in (b). The dashed lines are fits to the data points using the method described in the main text and Supporting Information S1. For $\Delta_0 > 0$ (blue), $\Delta_0 \approx 0$ (red), and $\Delta_0 < 0$ (black), average reaction rate k of 4.41×10^{-4} min^{-1} (blue), 2.39×10^{-4} min^{-1} (red), and 7.21×10^{-4} min^{-1} (black) are obtained, respectively. For clarify, the three sets of data points are offset to overlap at time zero.

Influences of mode detuning and coupling strength

Based on this quantification method, we systematically investigate the influence of mode detuning on the average reaction rates. Figure 3a shows the initial transmission spectra of a series of reactions with the same starting concentration of $[D_2O] = 0.2V_0$ but varying mode detuning values Δ_0. As the cavity length is reduced, the cavity mode blue shifts, resulting in a redistribution in the relative intensities of the upper (P^+) and lower (P^-) polariton peaks. Notably, this adjustment in the mode detuning value Δ_0 results in apparent changes in the reaction rates, as shown in Figure 3b: the reaction rate reduces and reaches a minimum when the cavity mode approaches that of the O-D vibrational mode at ~ 2500 cm^{-1} (i.e. $\Delta_0 \rightarrow 0$). The overall trend of the detuning-dependent reaction rate seems to follow the transmission spectrum of the O-D stretching mode, as was previously reported.[17, 20] This correlation between mode detuning and reaction rate can be consistently observed for reactions with different starting concentrations and consequently, coupling strength. Figure 3c-3d shows results from another set of reactions that have the same starting concentration of $[D_2O] = 0.5V_0$. A similar trend can be observed, with the reaction rate reducing to a minimum at zero detuning values. These findings clearly suggest the influence of mode detuning on the reaction rates. We would like to note that a further extension of mode detuning values to a broader range is restricted by the spacer thickness, free spectral range, and linewidth of the O-D vibrational mode.

For comparison, control experiments are also carried out under similar conditions using cell windows without coating the Au mirrors (termed as non-cavity). D_2O concentration-dependent non-cavity reaction rates are presented in Figure S6. Although slight variations in the non-cavity reaction rates are observed, there is no apparent D_2O concentration dependence, suggesting a change in the $[D_2O]$:[IPA] ratio has negligible influence on the reaction rate. We obtain an average non-cavity reaction rate of 5.56×10^{-6} min^{-1} (Figure 3b and 3d, dashed lines), which is slightly

larger than that reported in ref. [42]. Evidently, the inside-cavity reactions are accelerated compared to the non-cavity ones, with the acceleration extent varying for different D_2O concentrations. Specifically, when [D_2O] is increased from $0.2V_0$ to $0.5V_0$ (Figure 3b and 3d), which reflects an increase in the Rabi splitting from 242 cm^{-1} to 415 cm^{-1}, reaction acceleration can still be observed for the various detuning values, but apparently to a smaller extent.

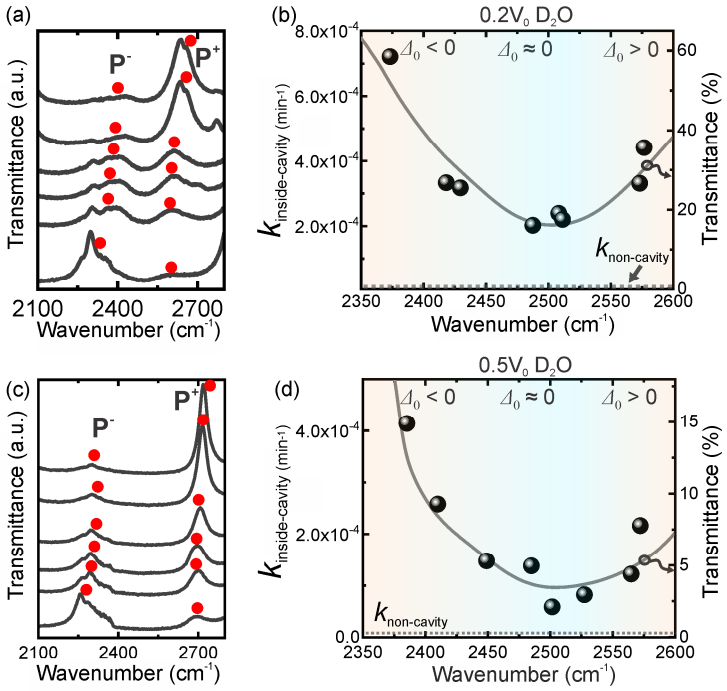

Figure 3. (a, c) FTIR transmittance spectra of reactions with initial D_2O concentrations of $0.2V_0$ (a) and $0.5V_0$ (c). (b, d) Reaction rates ($k_{\text{inside-cavity}}$) plotted as a function of the initial mode positions (i.e. $\boldsymbol{\omega_0} + \Delta_0$) for the $0.2V_0$ D_2O (b) and $0.5V_0$ D_2O (c) inside-cavity reactions. The rates are estimated utilizing the mode shift method. The gray solid lines represent the corresponding IR absorption spectra of the O-D stretching band. The dashed lines represent the average non-cavity reaction rates.

By defining $\mu = k_{\text{inside-cavity}}/k_{\text{non-cavity}}$ as the reaction rate acceleration factor, the effect of the coupling strength is further elucidated by plotting μ as a function of the Rabi splitting while keeping the detuning value at $\Delta_0 \approx 0$ (Figure 4a). An overall decrease in the acceleration factor, μ,

can be observed with increasing Rabi splitting. A 77-fold increase in the reactivity is observed for reactions with $[D_2O] = 0.1V_0$ (see Figure S7 for example spectra), while for reactions with $[D_2O] = 0.5V_0$, the average acceleration factor is reduced to only 15-fold, signifying the profound influence of coupling strength between the O-D stretching mode and cavity mode on the reaction rates.

The observations of minimum rates at $\Delta_0 \approx 0$ and decreasing rate acceleration factor μ with increasing Rabi splitting are to some extent supportive of the strong coupling-induced resonant effect predicted by several theoretical works. For instance, Schäfer et al.[38] have used quantum electrodynamical density functional theory to perform real-time simulations of a single strongly-coupled molecule, and found that the reaction trajectory was trapped in the local minimum due to strong coupling-assisted energy redistribution, leading to rate inhibition. By including the dipole self-energy term in the Shin-Metiu model, Li et al. also predicted that the molecular reaction coordinate can become trapped under resonant conditions, leading to a slowdown in the reaction.[36]

However, our observation of considerable acceleration at small Rabi splitting and large mode detuning suggests that a competing factor exists along with the resonant effect. In this regard, Du et al. recently proposed that the *N*-1 dark states existing in a strongly coupled system could enhance the thermalization rate, thus leading to reaction rate acceleration.[39] We would like to note, though, that the rate acceleration factor predicted in Ref. [39] is much smaller than the maximum values observed in this study, potentially due to different potential energy surfaces involved or other factors that render a direction comparison challenging (for instance, the recently reported ionic conductivity enhancement of water upon strong coupling of its O-H vibrational mode to a FP cavity).[47] Notably, dark state-mediated thermalization was also predicted by Li et al. using classical cavity molecular dynamics simulations.[40]

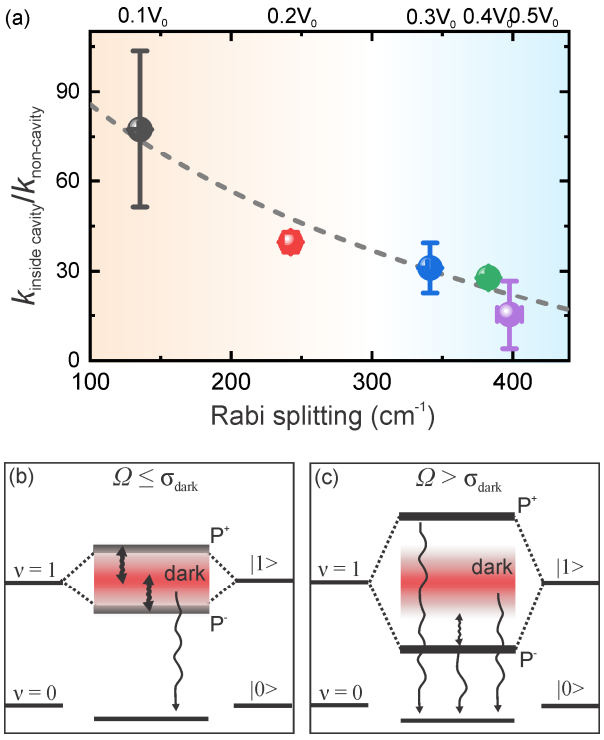

Figure 4. (a) Reaction rate ratios between inside-cavity and non-cavity reactions, $\mu = k_{\text{inside-cavity}}/k_{\text{non-cavity}}$, as a function of the Rabi splitting with $\Delta_0 \approx 0$. (b, c) Simplified sketches of population transfer and decay processes for different Rabi splitting, Ω. When Rabi splitting is smaller or comparable to the absorption linewidth of the vibrational mode (σ_{dark}) (b), the polaritonic bright states overlap substantially with the dark states. Notable population transfer between the bright and dark states occurs, followed by thermal dissipation. In this case, the dark state-mediated catalytic effect dominates. (c) For large Rabi splitting, namely $\Omega > \sigma_{\text{dark}}$, the polaritonic bright states are well isolated from the dark states. The polaritonic bright state-mediated resonant phenomenon becomes more important, which has an inhibiting effect on the reactivity. This leads to a reduced acceleration rate.

Based on our experimental findings and those earlier theoretical works, we propose a potential explanation for the simultaneous observation of rate acceleration and resonant effect in this reaction system. Specifically, we consider that the polaritonic bright and dark states contribute collectively to the overall reactivity. In a ground-state chemical reaction such as the one in this

study, vibrational energy relaxation and intermolecular energy transfer rates play an important role in the reaction rates.[40] Under vibrational strong coupling conditions, two polaritons and N-1 dark modes would be formed, constituting a highly nonequilibrium system. The bright polaritons predominantly result in reaction inhibition due to trapping of reaction trajectories under resonant conditions.[36, 38] On the other hand, the hot molecules in the dark mode reservoir have accelerated intermolecular vibrational energy transfer rates when compared to molecules in a non-cavity,[39, 40] thus resulting in catalytic effects on the thermally activated reaction studied here. As such, the overall reactivity of the system is determined by the competition between the opposite effects caused by the bright polariton and dark modes. Moreover, depending on the strong coupling conditions, the bright polaritons may primarily relax into the dark modes or directly to the ground state. This suggests that the contributions of the bright polariton and dark modes and the resultant overall reactivity are intimately related to the strong coupling conditions. At small Rabi splitting, Ω, and/or large mode detuning, dark states play a more important role due to their substantial overlap with the bright polaritonic states, such that the polaritons can readily dephase into the dark manifold[33, 34, 48, 49] followed by thermal dissipation (Figure 4b and S8b), which leads to a prominent acceleration. In contrast, at large Rabi splitting and/or small mode detuning, the resonant effect dominates over dark state-related thermalization due to small overlaps between the polaritonic bright and dark states, and a smaller acceleration effect (or even deceleration) may occur (Figure 4c and S8a). It is worth noting that earlier studies of this reaction system were carried out in the ultrastrong coupling regime.[43] Based on the observations in this study, a negligible catalytic effect in the ultrastrong coupling regime is plausible if the mechanisms governing polariton reactions in strong and ultrastrong coupling regimes are comparable.

Aside from Figure 4a, these speculations are also consistent with a weak correlation we observe between the polaritonic bright-dark overlap and the reaction rate (Figure S9). In these analyses, we use the bare D_2O molecules' absorbance to represent the energy distributions of the polaritonic dark states, and the integral of their spectral overlap with the cavity modes as the polaritonic bright-dark overlap. A larger overlap is generally associated with a faster reaction. We speculate that the large linewidth of the O-D stretching mode used in this study helps promote the influence of the dark states.[50, 51] While these findings in general support our speculations, the trend observed in Figure S9 is convoluted with the influence of the coupling strength. To further disentangle the effects of the polaritonic bright and dark states, carefully designed experiments would be required to rigorously test the effect of strong coupling on the thermal equilibrium of a reaction system.[40]

CONCLUSION

In summary, we find that the reactivity of the hydrolysis reaction studied here depends strongly on both cavity mode detuning and coupling strength. Depending on the coupling condition, different acceleration factors in the reaction rates are observed. In particular, the reaction rates decrease with increasing Rabi splitting and reach minima when in resonance with the cavity modes. While the Rabi splitting- and resonance-dependent reaction rates signify the contribution of polaritonic bright states in determining the reactivity,[36] the catalysis effect observed in the same system implies that changes in the thermalization rates upon VSC, likely associated with the dark states,[39] also affect the reactivity. Based on these results, we speculate that the overall reactivity of the VSC system investigated here is dependent on the intricate and collective effects of polaritonic bright and dark

states. Future studies with a focus on unveiling the thermalization rates of VSC systems could help further verify and discern the contributions of bright and dark states to chemical reactivities.

EXPERIMENTAL METHODS

Preparation and assembly of Fabry-Pérot (FP) cavities. Commercially available, 4 mm thick CaF_2 windows (Specac Ltd. UK) were subsequently coated with 10 nm Au, 2 nm Cr, and a 100 nm SiO_2 passivating layer using sputtering (AJA International Inc.). The microfluidic FTIR flow cell (GS20590 Series) and 6 μm-thick Mylar spacers were purchased from Specac Ltd. UK. A pair of CaF_2 windows separated by a 6 μm-thick Mylar spacer were assembled in the FTIR flow cell to form a FP cavity (Figure S1a-1b). The cavity length was fine adjusted using the four screws of the flow cell until desired resonance conditions were achieved. We then put a stainless steel mask with a hole diameter of 7.36 mm on the exterior of the front window (Figure S1b right).[52] A representative IR transmission spectrum of an as-assembled empty cavity is shown in Figure S1c. Typically, the as-assembled empty cavities were left to stand still for over 30 minutes before the subsequent operations.[53]

Monitoring the hydrolysis reaction in a cavity. At room temperature (~ 23 °C), 1 M ammonia borane solutions were prepared by dissolving ammonia borane (Sigma-Aldrich) into mixtures of D_2O (Sigma-Aldrich) and IPA (Sigma-Aldrich). After shaking the mixtures for several seconds, the solutions were immediately injected into the FP cavities. The flow cell was then sealed using Parafilm and the time used to seal the system was kept to less than 5 mins. After that, IR transmission spectra with a 2 cm^{-1} resolution and each with over 64 scans were recorded at constant

intervals (5 mins) using a standard FTIR spectrometer (Nicolet 6700). As the average refractive index of the products was smaller than that of the reactants, blue shifts of the cavity modes were observed during the reactions. As a comparison, non-cavity experiments were carried out following a similar procedure but using FTIR flow cells with CaF_2 windows coated with SiO_2 only without the Au and Cr layers.

To ensure accurate comparisons among various reactions, we restrict the use of data to those recorded over similar reaction time (0 - 25 min) and interval (5 min). Also, we perform all the reactions under continuous IR irradiation to make sure that they are subject to similar durations of IR exposure.

NMR Characterization. 480 μL solutions of ammonia borane (1 M) using H_2O and D_2O as the solvents, respectively, were used for the NMR measurements. After storing the solutions for 12 days, their ^{1}H and ^{11}B NMR spectra were taken with a Bruker NMR spectrometer, each using 120 μL dimethyl sulfoxide-d6 (Sigma-Aldrich) as the locking solvent.

Numerical simulations. The finite-difference time-domine (FDTD) method (Ansys) was used to simulate the electric field distributions inside a FP cavity. In a typical simulation, a Gaussian source was used to illuminate the cavity. PML and periodic boundary conditions were used for the directions perpendicular to and along the cavity. A mesh size of 10 nm was used for the cavity region.

ASSOCIATED CONTENT

Supporting Information. The following files are available free of charge. Description of the FP microcavity; NMR spectra of the reaction products; Reaction time-dependent IR spectra of control experiments; Derivation of the reaction rate from the cavity mode shifts; Reaction rates calculated using different modes; Concentration-dependent non-cavity reaction rates; An example of $0.1V_0$ D_2O reactions; Illustration of mode detuning dependent reactivity; Correlation between μ and polaritonic bright-dark overlap integral.

AUTHOR INFORMATION

Corresponding Author

*E-mail address: xuedan.ma@rice.edu

Notes

The authors declare no competing financial interests.

ACKNOWLEDGMENT

We acknowledge support from the National Science Foundation CBET Program under the award no. 2025214. Work performed at the Center for Nanoscale Materials, a U.S. Department of Energy Office of Science User Facility, was supported by the U.S. DOE, Office of Basic Energy Sciences, under Contract No. DE-AC02-06CH11357. X.M. acknowledges support from a startup grant from Rice University. We thank Ralu Divan for her help in preparing the flow cells windows.

Funding Sources

U.S. National Science Foundation CBET Program, award no. 2025214; U.S. Department of Energy, Office of Basic Energy Sciences, Contract No. DE-AC02-06CH11357; startup grant from Rice University.

REFERENCES

1. R. Bouchendira, P. Cladé, S. Guellati-Khélifa, F. Nez, F. Biraben. New Determination of the Fine Structure Constant and Test of the Quantum Electrodynamics. *Phys. Rev. Lett.* **106**, 080801 (2011)
2. J. Flick, M. Ruggenthaler, H. Appel, A. Rubio. Atoms and molecules in cavities, from weak to strong coupling in quantum-electrodynamics (QED) chemistry. *Proc. Natl. Acad. Sci.* **114**, 3026-3034 (2017)
3. J. D. Plumhof, T. Stöferle, L. Mai, U. Scherf, R. F. Mahrt. Room-temperature Bose–Einstein condensation of cavity exciton–polaritons in a polymer. *Nat. Mater.* **13**, 247-252 (2014)
4. J. Kasprzak, M. Richard, S. Kundermann, A. Baas, P. Jeambrun, J. M. J. Keeling, F. M. Marchetti, M. H. Szymańska, R. André, J. L. Staehli, V. Savona, P. B. Littlewood, B. Deveaud, L. S. Dang Bose–Einstein condensation of exciton polaritons. *Nature* **443**, 409-414 (2006)
5. K. M. Birnbaum, A. Boca, R. Miller, A. D. Boozer, T. E. Northup, H. J. Kimble Photon blockade in an optical cavity with one trapped atom. *Nature* **436**, 87-90 (2005)
6. H. J. Snijders, J. A. Frey, J. Norman, H. Flayac, V. Savona, A. C. Gossard, J. E. Bowers, M. P. van Exter, D. Bouwmeester, W. Löffler. Observation of the Unconventional Photon Blockade. *Phys. Rev. Lett.* **121**, 043601 (2018)
7. F. Ge, X. Han, J. Xu. Strongly Coupled Systems for Nonlinear Optics. *Laser Photonics Rev.* **15**, 2000514 (2021)
8. K. Wang, M. Seidel, K. Nagarajan, T. Chervy, C. Genet, T. Ebbesen. Large optical nonlinearity enhancement under electronic strong coupling. *Nat. Commun.* **12**, 1486 (2021)
9. P. Dombi, Z. Pápa, J. Vogelsang, S. V. Yalunin, M. Sivis, G. Herink, S. Schäfer, P. Groß, C. Ropers, C. Lienau. Strong-field nano-optics. *Rev. Mod. Phys.* **92**, 025003 (2020)
10. X. Zhong, T. Chervy, L. Zhang, A. Thomas, J. George, C. Genet, J. A. Hutchison, T. W. Ebbesen. Energy Transfer between Spatially Separated Entangled Molecules. *Angew. Chem. Int. Ed.* **56**, 9034-9038 (2017)
11. M. Du, L. A. Martínez-Martínez, R. F. Ribeiro, Z. Hu, V. M. Menon, J. Yuen-Zhou. Theory for polariton-assisted remote energy transfer. *Chem. Sci.* **9**, 6659-6669 (2018)

12. Garcia-Vidal, F. J., Ciuti, C., Ebbesen, T. W. Manipulating matter by strong coupling to vacuum fields. *Science* **373**, eabd0336 (2021)
13. M. Hertzog, M. Wang, J. Mony, K. Börjesson. Strong light–matter interactions: a new direction within chemistry. *Chem. Soc. Rev.* **48**, 937-961 (2019)
14. T. Schwartz, J. A. Hutchison, C. Genet, T. W. Ebbesen. Reversible Switching of Ultrastrong Light-Molecule Coupling. *Phys. Rev. Lett.* **106**, 196405 (2011)
15. J. Fregoni, G. Granucci, E. Coccia, M. Persico, S. Corni Manipulating azobenzene photoisomerization through strong light–molecule coupling. *Nat. Commun.* **9**, 4688 (2018)
16. B. Munkhbat, M. Wersäll, D. G. Baranov, T. J. Antosiewicz, T. Shegai. Suppression of photo-oxidation of organic chromophores by strong coupling to plasmonic nanoantennas. *Sci. Adv.* **4**, eaas955 (2018)
17. A. Thomas, J. George, A. Shalabney, M. Dryzhakov, S. J. Varma, J. Moran, T. Chervy, X. Zhong, E. Devaux, C. Genet, J. A. Hutchison, T. W. Ebbesen. Ground-State Chemical Reactivity under Vibrational Coupling to the Vacuum Electromagnetic Field. *Angew. Chem. Int. Ed.* **55**, 11462-11466 (2016)
18. R. M. A. Vergauwe, A. Thomas, K. Nagarajan, A. Shalabney, J. George, T. Chervy, M. Seidel, E. Devaux, V. Torbeev, T. W. Ebbesen. Modification of Enzyme Activity by Vibrational Strong Coupling of Water. *Angew. Chem. Int. Ed.* **58**, 15324-15328 (2019)
19. J. Lather, P. Bhatt, A. Thomas, T. W. Ebbesen, J. George. Cavity Catalysis by Cooperative Vibrational Strong Coupling of Reactant and Solvent Molecules. *Angew. Chem. Int. Ed.* **58**, 10635-10638 (2019)
20. A. Thomas, L. Lethuillier-Karl, K. Nagarajan, R. M. A. Vergauwe, J. George, T. Chervy, A. Shalabney, E. Devaux, C. Genet, J. Moran, T. W. Ebbesen. Tilting a ground-state reactivity landscape by vibrational strong coupling. *Science* **363**, 615-619 (2019)
21. K. Hirai, R. Takeda, J. A. Hutchison, H. Uji-i. Modulation of Prins Cyclization by Vibrational Strong Coupling. *Angew. Chem. Int. Ed.* **59**, 5332-5335 (2020)
22. W. Ahn , J. F. Triana, F. Recabal, F. Herrera, B. S. Simpkins. Modification of ground-state chemical reactivity via light–matter coherence in infrared cavities. *Science* **380**, 1165-1168 (2023)
23. D. S. Wang, S. F. Yelin. A Roadmap Toward the Theory of Vibrational Polariton Chemistry. *ACS Photon.* **8**, 2818-2826 (2021)
24. J. Fregoni, F. J. Garcia-Vidal, J. Feist. Theoretical Challenges in Polaritonic Chemistry. *ACS Photon.* **9**, 1096-1107 (2022)
25. J. Yuen-Zhou, W. Xiong, T. Shegai. Polariton chemistry: Molecules in cavities and plasmonic media. *J. Chem. Phys.* **156**, 030401 (2022)
26. T. E. Li, Z. Tao, S. Hammes-Schiffer. Semiclassical Real-Time Nuclear-Electronic Orbital Dynamics for Molecular Polaritons: Unified Theory of Electronic and Vibrational Strong Couplings. *J. Chem. Theory Comput.* **18**, 2774-2784 (2022)
27. D. S. Wang, T. Neuman, S. F. Yelin, J. Flick. Cavity-Modified Unimolecular Dissociation Reactions via Intramolecular Vibrational Energy Redistribution. *J. Phys. Chem. Lett.* **13**, 3317-3324 (2022)
28. D. S. Wang; J. Flick; S. F. Yelin. Chemical reactivity under collective vibrational strong coupling. *J. Chem. Phys.* **157**, 224304 (2022)
29. J. P. Philbin; Y. Wang; P. Narang; W. Dou. Chemical reactions in imperfect cavities: enhancement, suppression, and resonance. *J. Phys. Chem. C* **126**, 14908-14913 (2022)

30. L. P. Lindoy, A. Mandal, D. R. Reichman. Resonant Cavity Modification of Ground-State Chemical Kinetics. *J. Phys. Chem. Lett.* **13**, 6580-6586 (2022)
31. A. Mandal, M. A. D. Taylor, B. M. Weight, E. R. Koessler, X. Li, P. Huo. Theoretical advances in polariton chemistry and molecular cavity quantum electrodynamics. *Chem. Rev.* **123**, 9786-9879 (2023)
32. A. D. Dunkelberger, B. T. Spann, K. P. Fears, B. S. Simpkins, J. C. Owrutsky Modified relaxation dynamics and coherent energy exchange in coupled vibration-cavity polaritons. *Nat. Commun.* **7**, 13504 (2016)
33. B. Xianga, R. F. Ribeirob, A. D. Dunkelbergerc, J. Wangb, Y. Lia, B. S. Simpkinsc, J. C. Owrutskyc, J. Yuen-Zhoub, W. Xiong. Two-dimensional infrared spectroscopy of vibrational polaritons. *Proc. Natl. Acad. Sci.* **115**, 4845-4850 (2018)
34. G. Groenhof, C. Climent, J. Feist, D. Morozov, J. J. Toppari. Tracking Polariton Relaxation with Multiscale Molecular Dynamics Simulations. *J. Phys. Chem. Lett.* **10**, 5476-5483 (2019)
35. Y. Pang, A. Thomas, K. Nagarajan, R. M. A. Vergauwe, K. Joseph, B. Patrahau, K. Wang, C. Genet, T. W. Ebbesen. On the Role of Symmetry in Vibrational Strong Coupling: The Case of Charge-Transfer Complexation. *Angew. Chem. Int. Ed.* **59**, 10436-10440 (2020)
36. X. Li, A. Mandal, P. Huo. Cavity frequency-dependent theory for vibrational polariton chemistry. *Nat. Commun.* **12**, 1315 (2021)
37. A. Mandal, X. Li, P. Huo. Theory of vibrational polariton chemistry in the collective coupling regime. *J. Chem. Phys.* **156**, 014101 (2022)
38. C. Schäfer, J. Flick, E. Ronca, P. Narang, A. Rubio. Shining Light on the Microscopic Resonant Mechanism Responsible for Cavity-Mediated Chemical Reactivity. *Nat. Commun.* **13**, 7817 (2021)
39. M. Du, J. Yuen-Zhou. Catalysis by Dark States in Vibropolaritonic Chemistry. *Phys. Rev. Lett.* **128**, 096001 (2022)
40. T. E. Li, A. Nitzan, J. E. Subotnik. Collective Vibrational Strong Coupling Effects on Molecular Vibrational Relaxation and Energy Transfer: Numerical Insights via Cavity Molecular Dynamics Simulations. *Angew. Chem. Int. Ed.* **60**, 15533-15540 (2021)
41. R. Emmanuele, M. Maciejczyk, A. Smith, X. Cheng, E. Masson, D. J. Gosztola, S. W. Hla, N. Robertson, X. Ma. Microcavity-Modified Emission from Rare-Earth Ion-Based Molecular Complexes. *ACS Photon.* **9**, 2315-2321 (2022)
42. H. Hiura; A. Shalabney. Vacuum-Field Catalysis: Accelerated Reactions by Vibrational Ultra Strong Coupling. 2021, 7234721. *ChemRxiv.* *https://doi.org/10.26434/chemrxiv.7234721.v5*
43. M. V. Imperatore, J. B. Asbury, N. C. Giebink. Reproducibility of cavity-enhanced chemical reaction rates in the vibrational strong coupling regime. *J. Chem. Phys.* **154**, 191103 (2021)
44. Reichardt, C., *Solvents and Solvent Effects in Organic Chemistry, Third Edition*. 2002, Marburg, Germany: WILEY-VCH.
45. T. Yamashitaa, K. Takatsuka. Hydrogen-bond assisted enormous broadening of infrared spectra of phenol-water cationic cluster: An ab initio mixed quantum-classical study. *J. Chem. Phys.* **126**, 074304 (2007)

46. T. Fukushima, S. Yoshimitsu, K. Murakoshi. Vibrational Coupling of Water from Weak to Ultrastrong Coupling Regime via Cavity Mode Tuning. *J. Phys. Chem. C* **125**, 25832–25840 (2021)
47. T. Fukushima, S. Yoshimitsu, K. Murakoshi. Inherent Promotion of Ionic Conductivity via Collective Vibrational Strong Coupling of Water with the Vacuum Electromagnetic Field. *J. Am. Chem. Soc.* **144**, 12177-12183 (2022)
48. J. del Pino, J. Feist, F. J. Garcia-Vidal. Quantum theory of collective strong coupling of molecular vibrations with a microcavity mode. *New J. Phys.* **17**, 053040 (2014)
49. B. Xiang, R. F. Ribeiro, L. Chen, J. Wang, M. Du, J. Yuen-Zhou, W. Xiong. State-Selective Polariton to Dark State Relaxation Dynamics. *J. Phys. Chem. A* **123**, 5918-5927 (2019)
50. I. Diniz, S. Portolan, R. Ferreira, J. M. Gérard, P. Bertet, A. Auffèves. Strongly coupling a cavity to inhomogeneous ensembles of emitters: Potential for long-lived solid-state quantum memories. *Phys. Rev. A* **84**, 063810 (2011)
51. B. Cohn, S. Sufrin, A. Basu, L. Chuntonov. Vibrational Polaritons in Disordered Molecular Ensembles. *J. Phys. Chem. Lett.* **13**, 8369-8375 (2022)
52. Vergauwe, Robrecht M. A., Anoop Thomas, Kalaivanan Nagarajan, Atef Shalabney, Jino George, Thibault Chervy, Marcus Seidel, Eloïse Devaux, Vladimir Torbeev, and Thomas W. Ebbesen. Modification of Enzyme Activity by Vibrational Strong Coupling of Water. *Angewandte Chemie International Edition* **58**, 15324-15328 (2019)
53. Nagarajan, Kalaivanan, Anoop Thomas, and Thomas W. Ebbesen. Chemistry under Vibrational Strong Coupling. *Journal of the American Chemical Society* **143**, 16877-16889 (2021) 10.1021/jacs.1c07420.